Journal of Power Sources 196 (2011) 4671–4679

Contents lists available at ScienceDirect

Journal of Power Sources

journal homepage: www.elsevier.com/locate/jpowsour

Pumpless thermal management of water-cooled high-temperature proton exchange membrane fuel cells

Tae-Won Song, Kyoung-Hwan Choi*, Ji-Rae Kim, Jung S. Yi

Samsung Advanced Institute of Technology, Samsung Electronics Co. Ltd., Fuel Cell Group, Mt. 14-1, Nongseo-Dong, Giheung-Gu, Yongin-Si, Gyeonggi-Do 446-712, Republic of Korea

ARTICLE INFO

Article history:
Received 14 September 2010
Received in revised form 9 December 2010
Accepted 13 December 2010
Available online 18 January 2011

Keywords:
Proton exchange membrane fuel cell
Stack cooling
Latent heat
Dynamic characteristics
Pumpless

ABSTRACT

Proton exchange membrane fuel cells (PEMFCs) have been considered for combined heat and power (CHP) applications, but cost reduction has remained an issue for commercialization. Among various types of PEMFC, the high-temperature (HT) PEMFC is gaining more attention due to the simplicity of the system, that will make the total system cost lower. A pumpless cooling concept is introduced to reduce the number of components of a HT PEMFC system even further and also decrease the parasitic power required for operating the system. In this concept, water is used as the coolant, and the buoyancy force caused by the density difference between vapour and liquid when operated above boiling temperate is utilized to circulate the coolant between the stack and the cooling device. In this study, the basic parameters required to design the cooling device are discussed, and the stable operation of the HT PEMFC stack in both the steady-state and during transient periods is demonstrated. It found that the pumpless cooling method provides more uniform temperature distribution within the stack, regardless of the direction of coolant flow.

1. Introduction

Fuel cells are electrochemical power generation devices that directly convert chemical energy into electrical energy. Among various types of fuel cell, the proton exchange membrane fuel cell (PEMFC) has excellent characteristics, which are suited for transportation and small stationary and mobile applications [1]. On the other hand, because its typical operating temperature is below 100 °C, water management becomes an important issue to maintain the high activity of the membrane, while preventing dehydration of the proton conductor as well as flooding in the gas transport paths. When hydrocarbon fuels are used as the source of hydrogen, great care has to be taken to minimize catalyst poisoning by carbon monoxide.

To suppress the demerits of PEMFC, a high-temperature (HT) PEMFC, which operates above 100 °C, is gaining attention because there is no need of external humidification. Various attempts have been made to develop a new generation of organic proton conductors that can be used for HT PEMFC [2–7]. To date, polybenzimidazole (PBI)-based, phosphoric-acid doped membranes, which can work at 150–180 °C, are the only designs that have been established for commercial use [4–7]. The system eliminates components related to humidification. Also, high-temperature operation minimizes catalyst poisoning from reformed fuels and simplifies the components of the fuel reformer as compared in Fig. 1 [8]. In addition to its simplicity, the system provides improved system robustness along with higher quality heat for combined heat and power (CHP) applications. Overall HT PEMFC technology can be a cost-effective solution, especially when it is used with hydrocarbon-based fuel, where fuel reforming processes are required. Due to its nature of operating at high temperature, however, the thermal management of the stack becomes a greater concern [9].

Regarding the temperature control of HT PEMFCs, air cooling is an option, using a fan as a means to control the temperature of the stack [10–12]. Koh et al. [10] and Sohn et al. [11] investigated the influence of current density on the average cell temperature with an air-cooled stack and demonstrated that air cooling by natural convection was not sufficiently effective to maintain a uniform cell temperature. Peng and Lee [13] developed a 3D single-phase, non-isothermal numerical model for a single cell of HT PEMFC. The results showed that the thermal effects strongly affected the fuel cell performance and they suggested that active thermal management was strongly recommended, to maximize the performance of the stack.

For the use in CHP applications, liquid cooling, using water or oil has been widely adopted [14,15] due to the ease of heat recovery. Scholta et al. [15] investigated the external liquid cooling design of

* Corresponding author. Tel.: +82 31 280 8136; fax: +82 31 280 9359.
E-mail addresses: tw.song@samsumg.com (T.-W. Song), khchoi99@samsung.com (K.-H. Choi), jirae@samsung.com (J.-R. Kim), jungs.yi@samsung.com (J.S. Yi).

0378-7753/$ – see front matter © 2011 Elsevier B.V. All rights reserved.
doi:10.1016/j.jpowsour.2010.12.108

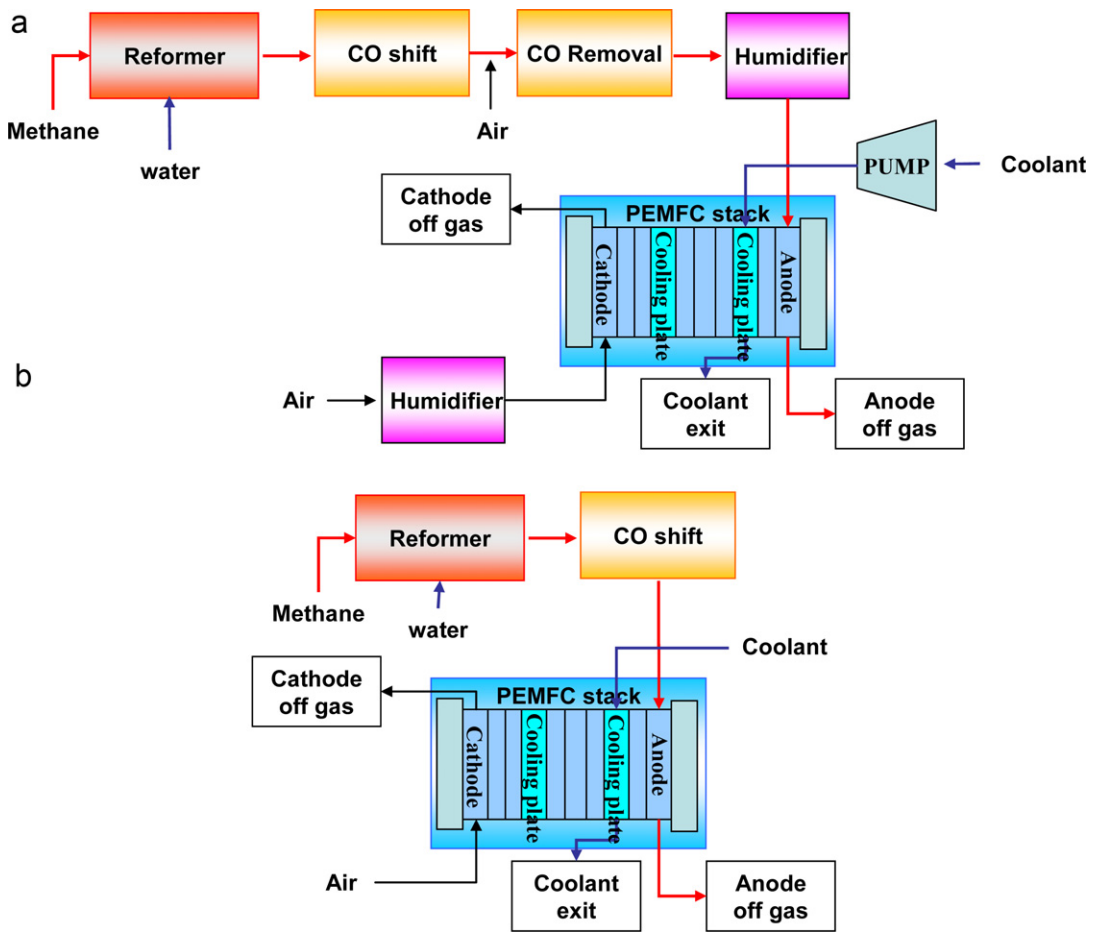

Fig. 1. Configurations of low and high temperature PEMFC systems; (a) low-temperature PEMFC system, (b) high-temperature PEMFC system.

HT PEMFC, wherein the cooling pipe went through the bipolar plate directly. It was shown that complete sealing of the cooling stream was feasible in the stack. Nevertheless, there existed the possibility of an improper contact between the cooling pipe and the bipolar plate that would result in lower cooling capability and would inevitably degrade the rate of heat transport. Moreover, it required electric insulation between the neighbouring bipolar plates for protection of short-circuit current through the cooling pipes.

Both air and liquid cooling methods require additional power to control the temperature of the stack [16,17]. Lee et al. [18] however, have suggested a pumpless stack cooling method, which can operate without the need of parasitic power for a circulating coolant. The method is suitable for an HT PEMFC, where the cell is operating at a temperature higher than the boiling temperature of the coolant, and it makes the best use of HT PEMFC with water as a coolant. Due to the phenomenon of the momentum generated from the density difference between the two co-existing phases, liquid and vapour, spontaneous water circulation between the stack and the cooling device can be obtained, without any external driving force, such as a pump. In this study, the feasibility of pumpless stack cooling of HT PEMFC is demonstrated. A cooling device for a 1 kWe HT PEMFC stack is designed, and it is found that pumpless operation is possible under both steady-state and transient conditions.

2. Stack cooling device of HT PEMFC

Heat generated in a fuel cell is inevitable due to reversible and irreversible chemical reactions. In typical PEMFCs, more than half of the chemical energy of fuel is converted to heat energy while generating electricity. For stable stack operation as well as high energy efficiency, it is important to design a cooling device properly to release heat from a fuel cell. In this study, a pumpless cooling device is designed for the thermal management of HT PEMFCs.

2.1. Heat transfer mechanism of HT PEMFC stack

The heat generated in a fuel cell stack should be delivered to the outside, therefore the coolant has to circulate through the channels of the cooling plates in a stack. The operating temperature of a low-temperature (LT) PEMFC is about 60–80 °C. Thus, a coolant such as air or water is usually supplied by a blower or pump, as shown in Fig. 1(a). Accordingly, the heat-transfer mechanism of a cooling plate in a LT PEMFC stack is forced convection using sensible heat. By contrast, a water-cooled HT PEMFC, which is operated at over 100 °C, contains additional latent heat that can provide enhanced cooling capability. Another merit of operating above the boiling temperature is that boiling generates pumping pressure for coolant circulation between the cooling plates and the cooling device to overcome the total pressure drop in the loop, which is the sum of frictional pressure drops in the cooling channel, connecting lines, and the heat-exchanger, plus any static pressure drop due to gravity. This pumping effect is caused by the density difference between the co-existing vapour phase and liquid phase (i.e., buoyancy effect) [16]. Therefore, no additional pump or blower is necessary, as shown in Fig. 1(b). In addition, the phenomenon of phase changing within the coolant stream causes the temperature of the cooling stream to remain unchanged, along the direction of the coolant flow, and there by helps to sustain a uniform cell

Nomenclature

A	heat-exchanger area/cm^2
c_p	specific heat at constant pressure/kJ kg^{-1} K^{-1}
D	diameter of coiled tube/m
d_i	inner diameter of pipe/m
F	Faraday constant (=96,485)/C mol^{-1}
g	acceleration of gravity (=9.81)/m s^{-2}
h	specific enthalpy/kJ kg^{-1}
$\bar{h}$	convective heat transfer coefficient/W m^{-2} K^{-1}
h_{fg}	latent heat energy/kJ kg^{-1}
I	current/A
Ja	Jakob number
k	thermal conductivity of coiled tube/W m^{-1} K^{-1}
k_c	thermal conductivity of secondary coolant/W m^{-1} K^{-1}
L	total length of coiled tube/m
N_{cell}	number of cells in the stack
N_{coil}	number of turns of the coil in heat-exchanger
$\overline{Nu}_D$	averaged Nusselt number
Q_c	flow rate of secondary coolant/L min^{-1}
$\dot{Q}_{conv}$	convective heat transfer to fuel and air gases/W
$\dot{Q}_{ele}$	electrical energy generated from the fuel cell/W
$\dot{Q}_{fuel}$	total enthalpy of supplied fuel/W
$\dot{Q}_{gen}$	generated heat from electrochemical reaction/W
$\dot{Q}_{rec}$	recovered heat by heat-exchanger/W
r	radius of tube/m
T_c	secondary coolant temperature/°C or K
T_s	surface temperature of coiled tube/K
T_{sat}	saturation temperature/K
V	stack voltage/V

Greek letters

μ	dynamic viscosity/kg m^{-1} s^{-1}
θ	angle between pipe and horizontal line/rad
ρ_c	density of secondary coolant/kg m^{-3}
ρ_l	density of liquid water/kg m^{-3}
ρ_v	density of vapour water/kg m^{-3}

Subscripts

c	secondary coolant
i	inlet
l	liquid water
o	outlet or outside
s	surface
sat	saturation
v	vapour water

temperature.

2.2. Thermal management using cooling device

Coolant water circulated through the stack goes to a cooling device where the excess heat is transferred to a secondary cooling stream. A cooling device for a HT PEMFC, as shown in Fig. 2, consists of a heat-exchanger, a reservoir and a solenoid valve. When the stack coolant exits the stack, the water in the liquid phase goes to the reservoir and the steam in the vapour phase goes to the heat-exchanger. A secondary coolant passes through the heat-exchanger to cool the steam of the stack coolant. The condensed water simultaneously enters from the reservoir to the cooling plate by the difference in water levels inside the reservoir and the cooling plate. At this time, the circulation of the stack coolant is achieved by natural convection as it boils inside the cooling channel, and a

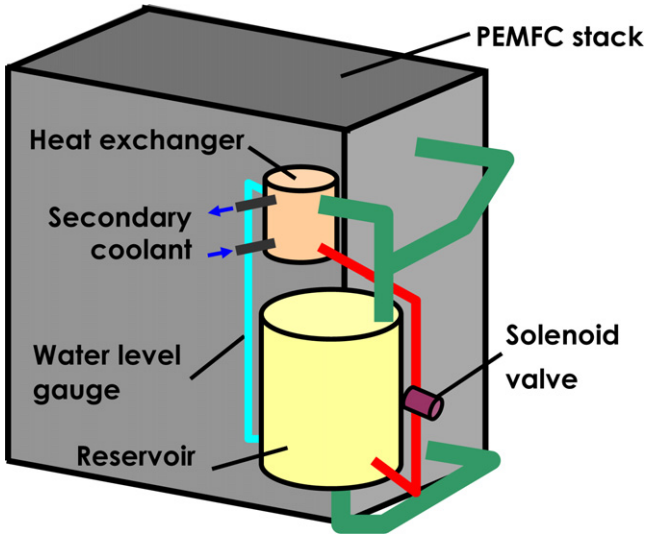

Fig. 2. Make-up of HT PEMFC stack and cooling device.

solenoid valve controls the operation of the heat-exchanger that affects the stack temperature as well as the secondary coolant outlet temperature.

During normal operation, the solenoid valve is opened to allow circulation of the condensed water in the heat-exchanger. When the temperature of the stack coolant entering into the heat-exchanger is lower than a set value, the solenoid valve is closed so that the heat-exchanger temperature is raised. Afterward, when the temperature of the stack coolant has increased to the desired level, the solenoid valve is opened so that the temperature can be maintained within the range set for stable operation.

2.3. Design of cooling device

Key targets in the design of a cooling device are the proper size and structure of the heat-exchanger. A helical coil structure of the heat-exchanger has been adopted due to its simplicity and generality [19]. In this section, the equations that describe the heat-transfer phenomena in the heat-exchanger, including the phase change, have been considered to determine the proper area of the heat-exchanger.

The amount of heat generated from the stack at a rated power, $\dot{Q}_{gen}$, can be calculated as shown in Eq. (1), where the electrical power generated from the fuel cell, $\dot{Q}_{ele}$ is subtracted from the total enthalpy of supplied fuel (e.g., hydrogen), $\dot{Q}_{fuel}$.

$$\dot{Q}_{gen} = \dot{Q}_{fuel} - \dot{Q}_{ele} = -\left(\frac{h}{2F} - V\right) \times I \times N_{cell} \quad (1)$$

here h is the specific enthalpy of fuel [kJ kg^{-1}], I and V are the mean current [A] and the voltage [V], respectively; F is the Faraday constant, 96,485(C mol^{-1}); N_{cell} is the number of cells in the stack. To design the heat-exchanger in a conservative manner, it is assumed that there is no heat loss to the outside. Subsequently, the amount of heat-exchanged in the heat exchanger, $\dot{Q}_{rec}$, can be expressed as:

$$\dot{Q}_{rec} = \dot{Q}_{gen} - \dot{Q}_{conv} \quad (2)$$

The second term of the right-hand side of Eq. (2) is the convective heat energy leaving the stack through the reactant streams of both the anode and the cathode.

In the heat-exchanger, the excess energy, $\dot{Q}_{rec}$, has to be transported from the stack coolant to the secondary coolant. The heat transport to the secondary coolant has to be proportional to the area of the heat-exchanger between the stack coolant and the secondary

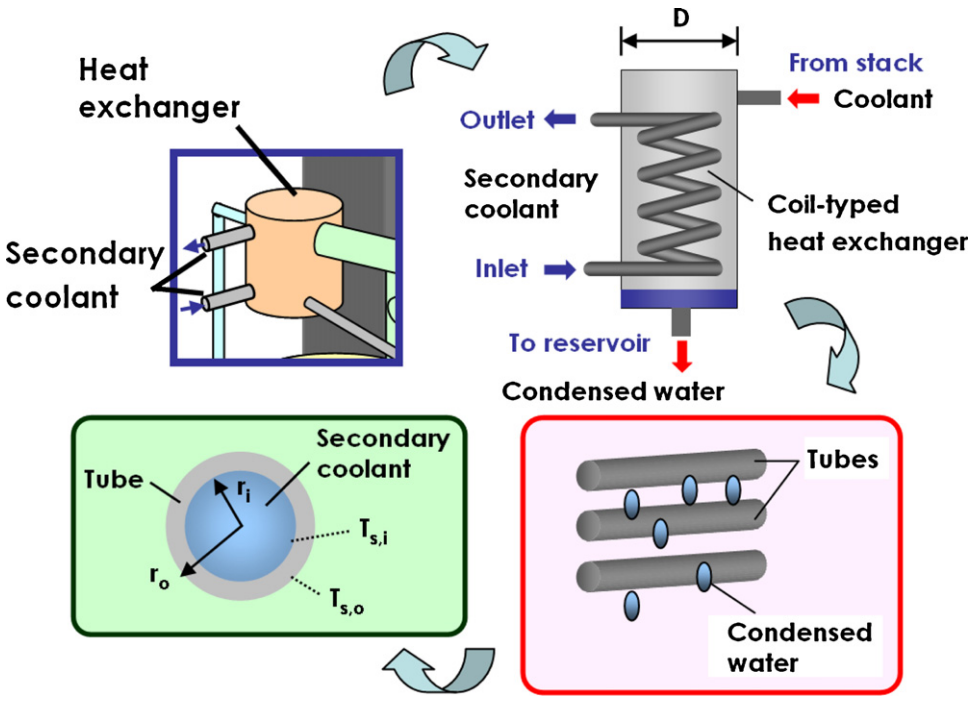

Fig. 3. A design of coil-typed heat-exchanger.

coolant, A, and it can be described as:

$$\dot{Q}_{rec} = \bar{h}_i A(T_s - T_c) \tag{3}$$

where $\bar{h}_i$ is the convective heat-transfer coefficient [W m^{-2}K^{-1}] of the inner side of the coil where the secondary coolant flows; T_s is the surface temperature [K] of the coil; T_c is the algebraic mean of the inlet temperature, $T_{c,i}$, and the outlet temperature, $T_{c,o}$, of the secondary coolant. The convective heat-transfer coefficient of the inner side of the coil, $\bar{h}_i$, is given by:

$$\bar{h}_i = \frac{\overline{Nu}_d k_c}{d_i} \tag{4}$$

here $\overline{Nu}_d$ is the averaged Nusselt number obtained from theoretical and experimental studies [20]. d_i and k_c are the inner diameter [m] of the coil and the thermal conductivity [W m^{-1} K^{-1}] of the secondary coolant, respectively.

At the surface of the coil, the energy from the stack coolant has to be identical to that of the secondary coolant of the heat-exchanger. Therefore, Eq. (3) can be rearranged as follows and in Fig. 3.

$$\begin{aligned}\dot{Q}_{rec} &= \bar{h}_i A_i = \bar{h}_i(2\pi r_i L)(T_{s,i} - T_c); \quad \text{inside of tube} \\ &= -kA\frac{dT_s}{dr} = \frac{2\pi kL}{\ln(r_o/r_i)}(T_{s,o} - T_{s,i}); \quad \text{tube} \\ &= \bar{h}_o A_o(T_{sat} - T_{s,o}) = \bar{h}_o(2\pi r_o L)(T_{sat} - T_{s,o}); \quad \text{outside of tube}\end{aligned} \tag{5}$$

where r_i and r_o are the radii [m] of inner and outer of the tube, respectively; L is the total length [m] of the tube; $T_{s,i}$ and $T_{s,o}$ are the surface temperatures [K] of the inner and the outer of the coiled tube [K]; k is the thermal conductivity [W m^{-1} K^{-1}] of the tube.

Using Eq. (5), the outer surface temperature of the tube can be calculated as:

$$T_{s,o} = \frac{(k/(\ln(r_o/r_i)) + \bar{h}_i r_i)\bar{h}_o r_o T_{sat} + k/(\ln(r_o/r_i))(\bar{h}_i r_i T_c)}{k/(\ln(r_o/r_i))(\bar{h}_i r_i + \bar{h}_o r_o) + \bar{h}_i r_i \bar{h}_o r_o} \tag{6}$$

where T_{sat} is the stack coolant temperature that is identical to the saturation temperature of steam [K]; $\bar{h}_o$ is the heat-transfer coefficient of condensation [W m^{-2}K^{-1}] of the outside of the coiled tube. On the outside surface of the tube, the stream changes to the liquid phase so that film condensation is considered to follow:

$$\bar{h}_o = C\left[\frac{g\cos\theta\rho_l(\rho_l - \rho_v)k_l{}^3 h'_{fg}}{N\mu_l(T_{sat} - T_{s,o})(2r_o)}\right]^{1/4} \tag{7}$$

$$h'_{fg} = h_{fg}(1 + 0.68\text{Ja}) \tag{8}$$

$$\text{Ja} = \frac{c_p(T_{sat} - T_{s,o})}{h_{fg}} \tag{9}$$

where C is 0.729 for a pipe [21], g is the acceleration of gravity [m s^{-2}]; ρ_l and ρ_v are the densities [kg m^{-3}] for liquid and vapour, respectively. k_l and μ_l are the thermal conductivity [W m^{-1} K^{-1}] and the viscosity [kg m^{-1} s^{-1}] for the liquid condensed on the surface of the coiled tube, respectively. N is the number of the paralleled pipes (i.e., the number of turns of the coil, N_{coil}); h_{fg} is the latent heat energy [kJ kg^{-1}]; θ is the angle between the pipe and the horizontal line. The corrected latent heat energy, h'_{fg} compensates for the heat transfer between the pipe and the condensed film. Ja, which is called the Jakob number, is the ratio of the absorbed sensible heat to latent heat. For a given diameter of tube and a given diameter of coiled tube, N_{coil} can be calculated as follows.

$$N_{coil} = \frac{A_o}{(2\pi r_o)\cdot(\pi DL)} \tag{10}$$

where D is the diameter [m] of the coiled tube.

By combining Eqs. (4)–(10) into Eq. (5), the heat-exchange area (i.e., the outer area of the coiled tube), A_o, can be calculated. As N_{coil} also depends on this area, it is necessary for the iterative calculation to identify the required heat-exchange area.

For the required amount of heat-exchange, the flow rate of the secondary coolant, Q_c [L min^{-1}] can be calculated as follows.

$$Q_c = \frac{\dot{Q}_{rec}}{\rho_c c_p(T_{c,o} - T_{c,i})} \tag{11}$$

where c_p is the specific heat [kJ kg^{-1} K^{-1}] at constant pressure; $T_{c,o}$ is generally set to a desired temperature, which is about 60 °C

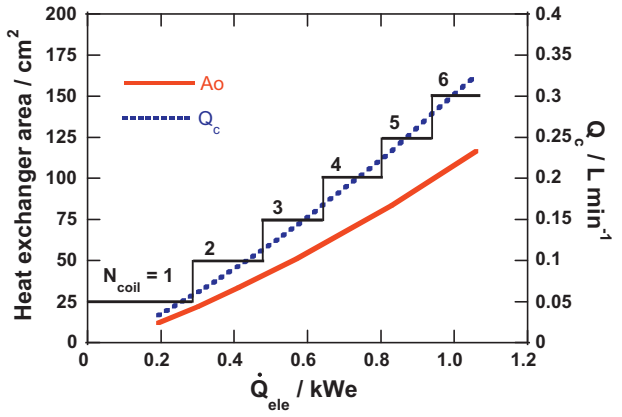

Fig. 4. Estimation of required heat-exchanger area, A_o (plain line), number of turns of coil, N_{coil} (step line), and flow rate of secondary coolant, Q_c (dotted line) for various electrical powers from 0.2 to 1.0 kWe.

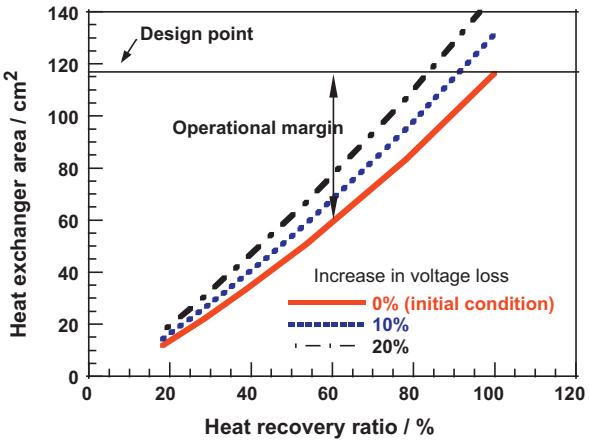

Fig. 5. Effect of heat recovery ratios and cell voltages on required heat-exchanger area. Increase in voltage loss due to cell degradation causes much higher heat generation and larger heat-exchanger area is required.

for the use of heat for CHP applications such as a heat-up water reservoir or heating buildings [22,23].

The required area of heat-exchanger for various levels of electrical output is shown in Fig. 4. The design point of the stack performance is taken to be 0.7 V at 0.2 A cm^{-2}. Fig. 4 also displays the number of turns of the coil, using the basic specifications of the heat-exchanger described in Table 1, and the required flow rate of the secondary coolant is also plotted. If 100% heat recovery from the cooling device is assumed, the required heat-exchanger area for a 1 kWe HT PEMFC is about 117 cm^2. When the shape of the coil shown in Table 1 is applied, it should have six turns of the coil to give the required heat-exchanger area. Then the flow rate of the secondary coolant should be 0.33 L min^{-1}. In practice, the heat recovery ratio will be lower than 100%. Therefore, the actual heat-exchanger area required will be smaller than 117 cm^2. If we assume the heat recovery ratio to be 85%, the required heat-exchanger area becomes about 93 cm^2 (see Fig. 5). As the cooling device has a heat-exchange area of 117 cm^2, it can be stated that more than 25% of the area is over-designed when the assumed heat recovery of the system is 85%. Another factor to be considered is that as fuel cell performance decays with time (i.e., cell voltage losses, such as ohmic and proton transport losses, increase gradually), the heat generated at the stack will be increased, and a greater heat-exchanger area will be required to handle the excess heat-generated. With the size of the heat exchanger considered a little earlier in the text, it can be estimated that the cooling capacity will be sufficient up to a 20% voltage loss (at 20 A) when at 85% heat recovery ratio is assumed (see Fig. 5).

Table 1
Design parameters of cooling device for 1 kWe HT PEMFC stack.

	Parameter	Value
Given	Saturation temperature (°C)	150
	Thermal conductivity of coil (W m^{-1} K^{-1})	15.6
	Diameter of coiled tube, D (mm)	40
	Outer radius of tube, r_o (mm)	2.5
	Inner radius of tube, r_i (mm)	1.8
	Temperature of secondary coolant (°C)	
	Inlet, $T_{c,i}$	20
	Outlet, $T_{c,o}$	60
Obtained	Number of turns of coil, N	6
	Heat-exchanger area, A_o (cm^2)	117
	Flow rate of secondary coolant, Q_c (L min^{-1})	0.33

3. Experimental set-up

Samsung Electronics is developing a micro-CHP system for residential applications using a HT PEMFC stack [24]. Phosphoric acid-doped hydrocarbon-based polymer membrane technology is adopted for operation at 150 °C. In-house developed high-performance MEAs (Membrane Electrode Assembly) are prepared using proprietary hydrocarbon membranes. Reactant flow channels and the layout of the bipolar plates are designed based on computational fluid dynamics analysis to maximize the power density while maintaining the fuel efficiency of the MEA. Detailed information of design and operation of the developed stack is as follows.

- Number of cells: 84.
- Active area of MEA: 100 cm^2.
- Utilization factor: 0.80 (fuel–hydrogen), 0.50 (air–oxygen).
- Gas pressure: atmosphere.
- Coolant (water) saturation pressure: about 0.5 MPa.
- Membrane: polybenzimidazole (PBI)-based polymer membrane.
- Electrode (catalyst): Pt/Ru (anode), Pt/Co (cathode).
- End plate: metal(stainless steel) and composite.
- Flow field design: straight type for fuel (hydrogen), air and coolant (water).
- Cooling plates located between each six cells.
- Internal manifold for fuel (hydrogen), air and water.

A cooling device with a size of 117 cm^2 was designed and attached to a 1 kWe class PEMFC stack. The temperature measurement points of the cooling device and the stack are indicated in Fig. 6. The stack exit temperature (T_{sat}) of the coolant was set at 150 °C. All temperatures of the bipolar plates (BP) in the stack were measured. The temperatures of the cooling plates (CP), especially, were measured at three points (bottom, middle, and top) along the direction of coolant flow.

4. Results and discussion

4.1. Testing at steady-state conditions

The stack combined with the cooling device, as described in Section 3, was tested up to 1 kWe to demonstrate that the cooling device could successfully maintain the stack temperature. Fig. 7 shows the stack voltages at various applied electrical currents, together with the averaged stack temperatures. Within a current range of 6–20 A, where the equivalent power output varies from 0.3

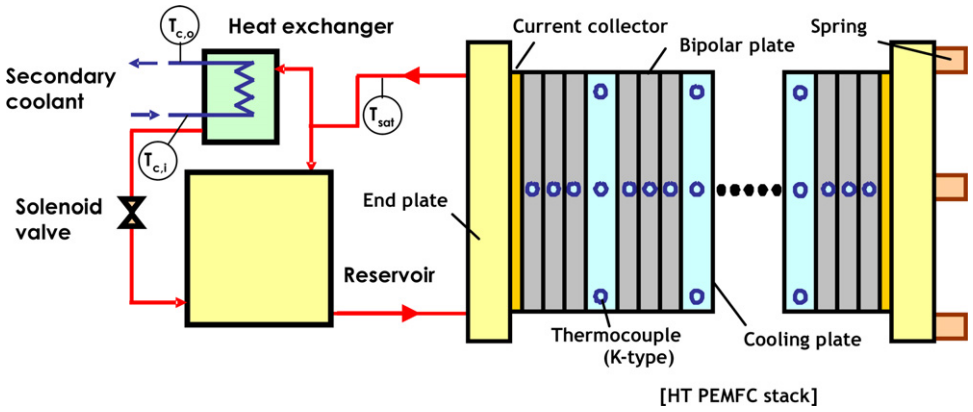

Fig. 6. Schematic diagram of cooling device for HT PEMFC stack.

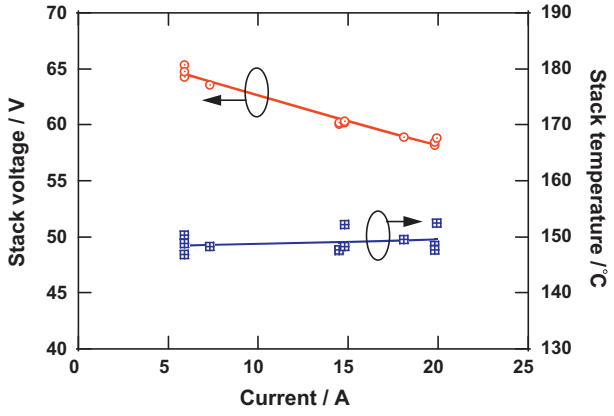

Fig. 7. Stack polarization curve and stack temperature at various electrical current. For stack safety, experiment under taken within ohmic-loss dominant range where cell voltage linearly decreases with current.

to 1.0 kWe, the stack temperature is stable at around 150 °C with an insignificant change (±3 °C), and the results are reproducible. The stack temperatures are the arithmetic average of the measured values at the centre positions of the bipolar plates.

The cell voltage distribution and the temperature distribution at a rated load of 20 A are presented in Fig. 8. The temperatures are measured at the middle position of a side of the cooling plate and at the middle position of the central bipolar plate, located between the two cooling plates. Because the measuring point of the cell temperature switches between the cooling plate and the bipolar plate,

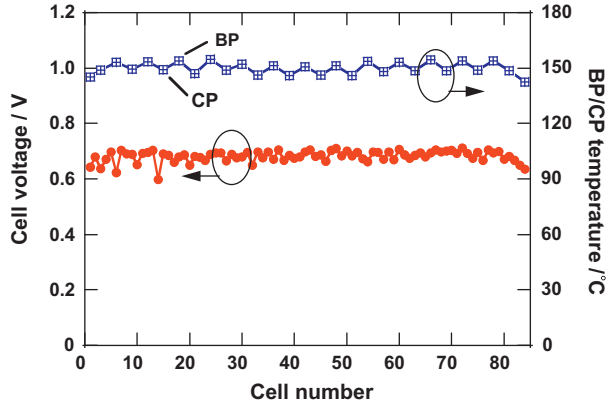

Fig. 8. Distribution of cell voltage and temperatures of bipolar and cooling plates at 20 A.

the temperature profile shows a systematic up-down trend within the stack. Higher values are the temperatures of the bipolar plates, and lower ones are those of the cooling plates. Within the range, the temperatures are evenly distributed, unlike in the case of using a pump or blower circulating coolant, where a temperature gradient is unavoidable. The reason for the uniform distribution of the stack temperature is the phase-change characteristic of saturated vapour, where the temperature is kept constant during the heat absorption process. Unlike the uniformity of most cells located between the cooling plates, there is a drop in the temperature profile at both ends of the stack. The convective heat loss to the ambient through the end-plates is significantly high such that the rates of heat conduction through the bipolar plates and coolant circulation near the end-plates are not sufficient to maintain a uniform temperature in the plates near the ends of the stack. This problem can be mitigated by improving the thermal insulation of the end-plates. To investigate the temperature profile in more detail, the temperatures of the cooling plates measured at three different locations (bottom, middle, and top) are shown in Fig. 9. The lowest temperature is the one at the bottom of the first cooling plate, where the coolant comes into the stack. Ideally, the incoming coolant temperature should be identical to the temperature within the stack. The convective heat loss through the cooling device however, makes the incoming coolant temperature cooler than the others. This should be related to the heat recovery ratio discussed later. Once the coolant water comes into the stack at about 10 °C lower, its temperature rises quickly to the stack temperature within and between the cooling plates. Except for the bottom temperature of the first coolant plate, the temperature distribution along the direction of coolant flow is uniformly maintained, regardless of the direction of the coolant flow. This demonstrates that the buoyancy-driven pumpless coolant circulation is not only able to eliminate the need of a pump, but can also ensure uniform temperature distribution along the stack. This will offer another competitive advantage of the HT PEMFC system, when applied with a pumpless cooling scheme, over a LT PEMFC-based CHP system.

The heat recovery ratio, that is, the ratio of the recovered heat to the generated heat from the stack, when various currents are applied is given in Fig. 10. A high heat recovery ratio can be obtained when the electrical current is higher than 7 A. At 6 A or lower currents, however, the heat recovery ratio drops to ~40%, while maintaining the temperature of the bipolar plates at the set value (see Fig. 7). This should be a critical heat generation condition where the convective heat loss to the ambient becomes relatively significant. The remaining thermal energy in the coolant stream is not sufficient to circulate the coolant from the stack to the cooling device, and therefore the excess heat recovered in the secondary coolant stream significantly decreases. Nevertheless, the momen-

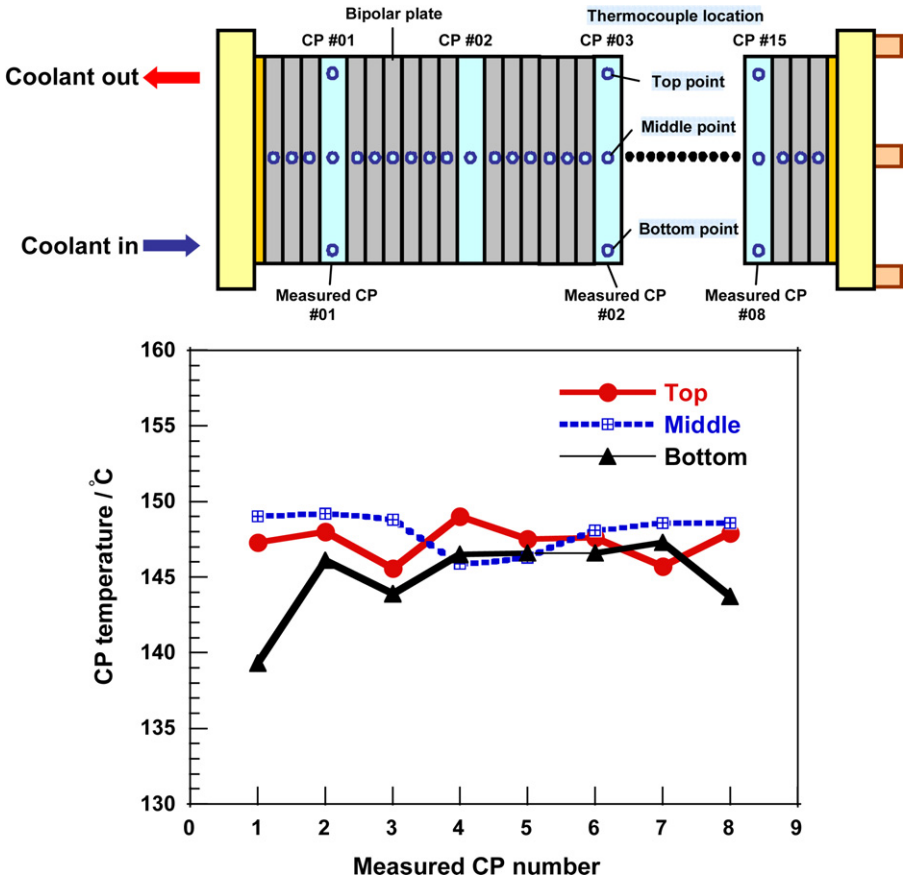

Fig. 9. Distribution of cooling plate temperatures along direction of coolant flow.

tum of circulation of the coolant within the stack is sufficient; for, the stack temperature to be maintained at approximately 150 °C, as shown in Fig. 7. With improved insulation of the stack as well as the cooling device, the critical current to maintain high thermal efficiency can be widened to lower current conditions.

4.2. Temperature control scheme of pumpless cooling operation

A cooling device should work within the wide range of generated heat following the part-load operation of the fuel cell stack. In this scheme, instead of using a pump, the flow rate of the condensed coolant water returned to the reservoir is controlled by the ON/OFF interval of the solenoid valve, as shown in Fig. 2. The configuration of the control part; a solenoid valve, a temperature controller, and a timer is illustrated in Fig. 11. The control mechanism of the stack temperature is simplified as shown in Fig. 12. Under the setting value of the stack temperature, all the components remain off. Over the setting value, the temperature controller begins to operate, and the timer gives the ON/OFF signal to the solenoid valve periodically. If the stack temperature decreases under the setting value, the tem-

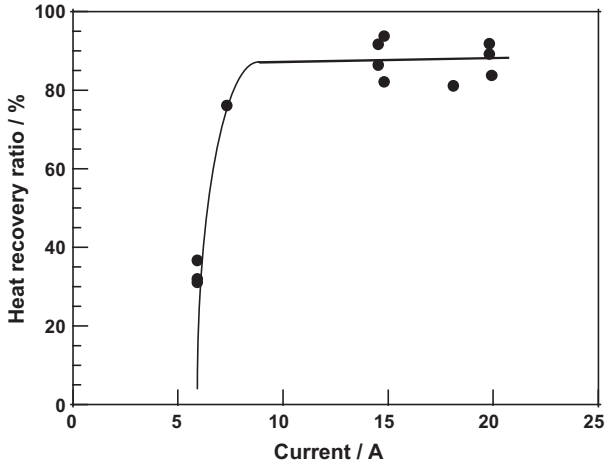

Fig. 10. Heat recovery ratio at various current conditions.

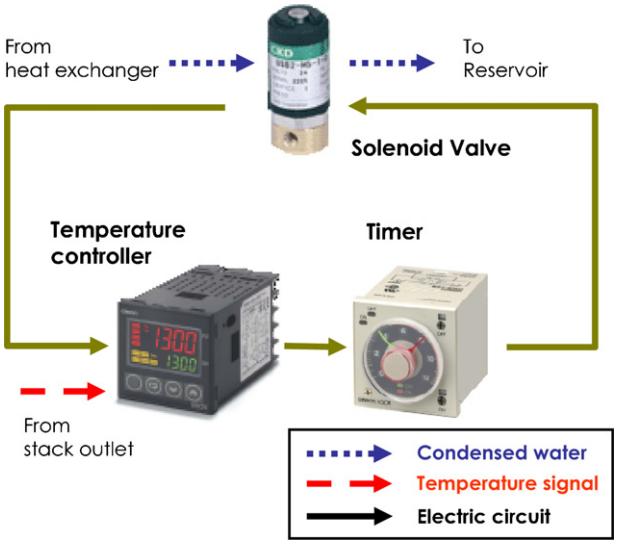

Fig. 11. Configuration of control part of cooling device for HT PEMFC stack.

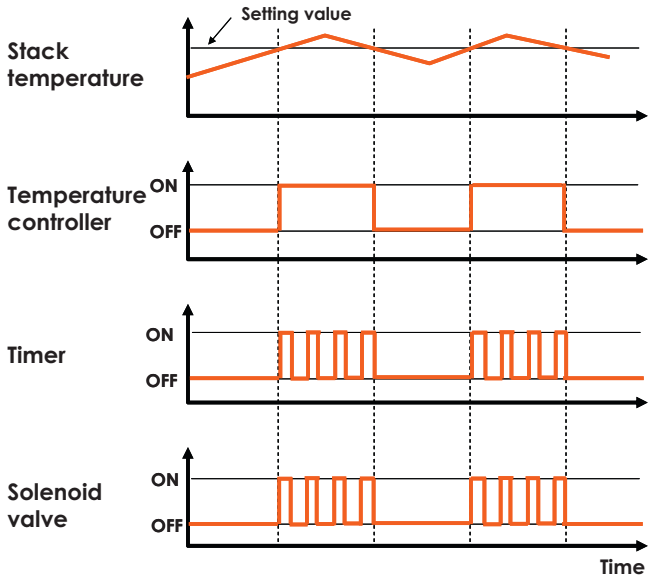

Fig. 12. Control mechanism of cooling device for HT PEMFC.

perature controller opens the circuit of the control part. The thermal controller controls the solenoid valve. To increase the stability and the controllability of the temperature, however, a timer is added as an additional controller, which controls the ON/OFF frequency of the solenoid valve depending on the level of electrical power applied to the stack.

It is important to understand exactly the characteristic of the ON/OFF interval of the solenoid valve for reliable stack operation. The fluctuations of the stack temperature and the outlet temperature of the secondary coolant are shown in Fig. 13. The stack temperature is much less sensitive to the energy change in the coolant than the secondary coolant temperature, due to the high thermal inertia of the stack (mainly, bipolar plates). Thus, it could be much more precise to sense the outlet temperature of the secondary coolant for control of the stack temperature. The influence of the periodic fluctuation of the outlet temperature of the secondary coolant can be analyzed in more detail, as shown in Fig. 14; region ① is the section where the solenoid valve is closed, and region ② is the one where the solenoid valve remains open, according to the ON/OFF interval set of the timer. By properly turning the ON/OFF interval, both the stack temperature and the outlet temperature of the secondary coolant can be maintained stable over the period of operation. Fig. 15 represents the characteristic of the

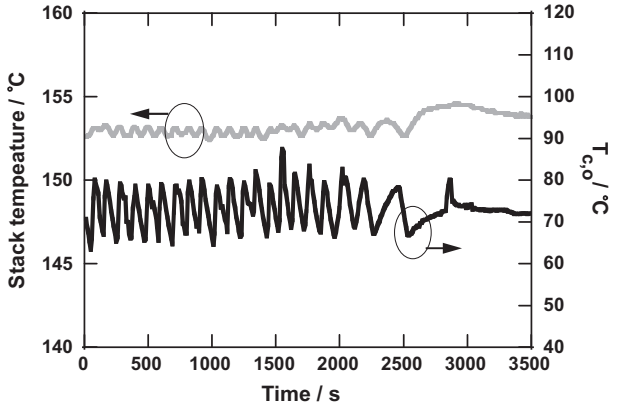

Fig. 13. Responses of stack temperature and secondary coolant outlet temperature at 20 A.

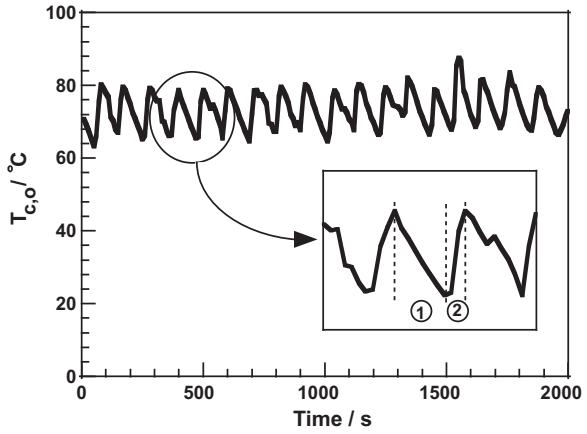

Fig. 14. Dynamic characteristics of secondary coolant outlet temperature in ON/OFF condition of solenoid valve.

ON/OFF interval of the solenoid valve. An increase in the OFF time of the solenoid valve mitigates the increase rate of the outlet temperature of the secondary coolant (region ①). It can prolong the stabilization time, but the amplitude of the variation of the outlet temperature of the secondary coolant does not change very much. Next, the ON time of the solenoid valve was set to decrease at region ② , decreasing the flow rate of the condensed water returning to the reservoir. Subsequently, the performance of the heat-exchanger goes down, and the amplitude of the variation of the outlet temperature of the secondary coolant also decreases, as shown in region ② . As demonstrated in Fig. 15, stable operation can be obtained by decreasing the ON time and increasing the OFF time. The 'hump' at around 2900s shown in Fig. 15(b) is caused by the instability in the supply of city water, which is not related to this study; in spite of an abrupt interruption of the secondary coolant temperature, the control scheme still can still maintain stable temperatures in the stack and the secondary coolant. The characteristic of the ON/OFF interval of the solenoid valve is summarized in Table 2.

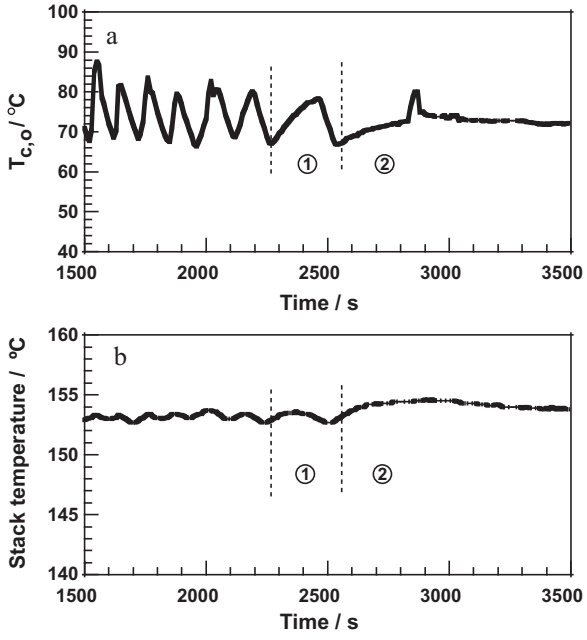

Fig. 15. Responses of (a) secondary coolant outlet temperature and (b) stack temperature with modulation of ON/OFF interval of solenoid valve.

Table 2
Characteristics according to ON/OFF interval of solenoid valve.

Time		Amplitude	Period
ON	OFF		
const	↑	const	↑
↓	const	↓	const

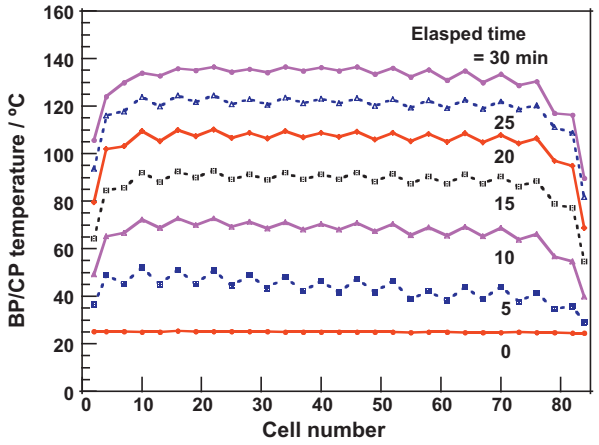

Fig. 16. Distribution of temperatures of bipolar and cooling plates during warming-up of HT PEMFC stack.

4.3. Transient capability during start-up period

A fuel cell stack should be heated up to some temperature before load operation [9,16]. In general, a heater directly warms up a fuel cell stack, or a heated coolant is supplied to it. In this study, the same mechanism as cooling is applied to the start-up, that is, the usage of natural convection without an external driving force, like a pump. The same control method using a solenoid valve is applied, as discussed in the previous section. The coolant circulates between the stack and the cooling device. The start-up heater is located in the reservoir. Fig. 16 shows the temperature distributions during warm-up of the stack. In the beginning (5–10 min), the temperature in the vicinity of the coolant inlet becomes relatively higher. The peak indicates the temperature of the cooling plate and the valley of the bipolar plate. A high-temperature coolant transfers heat from the cooling plate to the bipolar plate by convection and conduction. The temperature of the cooling plate along the stack can be kept uniform thus conforming reliable start-up with the pumpless cooling device with the control scheme, as discussed in the previous section. This demonstrates that transient operation with the pumpless cooling device is possible for a 1 kWe HT PEMFC stack.

5. Conclusions

A stack cooling device for a high-temperature (above 100 °C) PEMFC has been designed. It is operated using the phase-change latent heat of water without any external driving power. The designed cooling device is verified by demonstrating the stable operation of a 1 kWe class HT PEMFC stack. The results of the experiment show that the stack temperature can be kept within ±3 °C of the target temperature and its heat recovery ratio is up to 80% or higher. The dynamic characteristics have also been checked by solenoid valve control and it is seen that a stable operation can be obtained by adjusting the ON/OFF interval of the valve.

References

[1] S. Srinivasan, R. Mosdale, P. Stevens, C. Yang, Rev. Energy Environ. 24 (1999) 281–328.
[2] H. Tang, Z. Wan, M. Pan, S.P. Jiang, Electrochem. Commun. 9 (2007) 2003–2008.
[3] E.I. Santiago, R.A. Isidoro, M.A. Dresch, B.R. Matos, M. Linardi, F.C. Fonseca, Electrochim. Acta 54 (2009) 4111–4117.
[4] J.A. Asensio, S. Borros, P.G. Romero, J. Electrochem. Soc. 151 (2004) A304–A310.
[5] J. Zhang, Z. Xie, J. Zhang, Y. Tang, C. Song, T. Navessin, Z. Shi, D. Song, H. Wang, D.P. Wilkinson, Z.S. Liu, S. Holdcroft, J. Power Sources 160 (2006) 872–891.
[6] J.C. Wannek, B. Kohnenl, H.F. Oetjen, H. Lippert, J. Mergel, Fuel Cells 8 (2008) 87–95.
[7] Q.F. Li, J.O. Jensen, R.F. Savinell, N.J. Bjerrum, Prog. Polym. Sci. 34 (2009) 449–477.
[8] Q.F. Li, J.A. Gao, R.H. He, J.O. Jensen, N.J. Bjerrum, J. Electrochem. Soc. 150 (2003) A1599–A1605.
[9] S.G. Kandlikar, Z. Lu, Appl. Thermal Eng. 29 (2009) 1276–1280.
[10] J.H. Koh, A.T. Hsu, H.U. Akay, M.F. Liou, J. Power Sources 144 (2005) 122–128.
[11] Y.J. Sohn, G.G. Park, T.H. Yang, Y.G. Yoon, W.Y. Lee, S.D. Yim, C.S. Kim, J. Power Sources 145 (2005) 604–609.
[12] K.P. Adzakpa, J. Ramousse, Y. Dube, H. Akremi, K. Agbossou, M. Dostie, A. Poulin, M. Fournier, J. Power Sources 179 (2008) 164–176.
[13] J. Peng, S.J. Lee, J. Power Sources 162 (2006) 1182–1191.
[14] H.I. Lee, C.H. Lee, T.Y. Oh, S.G. Choi, I.W. Park, K.K. Baek, J. Power Sources 107 (2002) 110–119.
[15] J. Scholta, M. Messerschmidt, L. Jorissen, C. Hartnig, J. Power Sources 190 (2009) 83–85.
[16] S.J. Andreasen, S.K. Kaer, Int. J. Hydrogen Energy 33 (2008) 4655–4664.
[17] P. Pfeifer, C. Wall, O. Jensen, H. Hahn, Fichtner, Int. J. Hydrogen Energy (2009) 3457–3466.
[18] S.J. Lee, D.Y. Seung, T.W. Song, US2008/0050628.
[19] F.P. Incoprera, D.P. DeWitt, Fundamentals of Heat and Mass Transfer, 4th ed., John Wiley & Sons, Inc., New York, 1996.
[20] K. Sadik, K.S. Ramesh, A. Win, Handbook of Single-Phase Convective Heat Transfer, Chapter 5. Convective Heat Transfer in Curved Ducts, John Wiley & Sons, Inc., New York, 1987.
[21] V.K. Dhir, J.H. Lienhard, J. Heat Transfer 93 (1971).
[22] G. Gigliucci, L. Petruzzi, E. Cerelli, A. Garzisi, A. La Mendola, J. Power Sources 131 (2004) 62–68.
[23] H.S. Chu, F. Tsau, Y.Y. Yan, K.L. Hsueh, F.L. Chen, J. Power Sources 176 (2008) 499–514.
[24] J.S. Yi, K.H. Choi, S.W. Choi, J.S. Heo, S.G. Hong, J.R. Kim, J.O. Park, T.W. Song, H.Y. Sun, H. Chang, Fuel Cell Seminar and Exposition, California, USA, 2009.